frontiers in Earth Science

ORIGINAL RESEARCH
published: 09 March 2022
doi: 10.3389/feart.2022.856290

Molecular Dynamics Simulation of the Nanoindentation of Coal Vitrinite

Hewu Liu[1,2]*, *Chenliang Hou*[3] *and Yu Song*[3]*

[1]State Key Laboratory of Mining Response and Disaster Prevention and Control in Deep Coal Mines, Anhui University of Science and Technology, Huainan, China, [2]School of Earth and Environment, Anhui University of Science and Technology, Huainan, China, [3]School of Resources and Earth Science, China University of Mining and Technology, Xuzhou, China

Coal deformation is closely correlated with the distribution of organic maceral groups, however, molecular dynamics (MD) simulations of vitrinite nanoindentation have rarely been conducted. In this study, the vitrinite substrate for indentation was constructed utilizing polymer consistent force field (PCFF), and a spherical ghost indenter was used for loading. The results showed that: 1) In the indentation process, some of the vitrinite atoms overcame the energy barrier to move, with the most important deformation mechanism including the sliding, bending, and reorientation of vitrinite molecular chains, leading to the formation of a shearing transformation zone (STZ), which was also found to contain structural defects and stacking of aromatic structures. 2) The distribution of atomic displacements in the vitrinite substrate could be subdivided into distinct regions, with slippage at the region boundaries producing shear bands. 3) The surface morphology and mechanical properties obtained from the nanoindentation simulation were similar to experimental results from the literature, indicating that MD simulations are a powerful tool for studying coal nanoindentation. The results from this study increase the current scientific understanding of the mechanical properties of vitrinite by providing a new perspective that elucidates the nanoscale structural evolution occurring during the indentation process.

Keywords: nanoindentation, vitrinite, molecular dynamics simulation, molecular structure, mechanical properties

OPEN ACCESS

Edited by:
Jienan Pan,
Henan Polytechnic University, China

Reviewed by:
Junqing Meng,
China University of Mining and Technology, China
Anmin Wang,
China University of Mining and Technology, China

***Correspondence:**
Hewu Liu
hwliu65@163.com
Yu Song
songyu10094488@126.com

Specialty section:
This article was submitted to Economic Geology, a section of the journal Frontiers in Earth Science

Received: *17 January 2022*
Accepted: *21 February 2022*
Published: *09 March 2022*

Citation:
Liu H, Hou C and Song Y (2022) Molecular Dynamics Simulation of the Nanoindentation of Coal Vitrinite. Front. Earth Sci. 10:856290. doi: 10.3389/feart.2022.856290

1 INTRODUCTION

As a type of organic rock, coal is very sensitive to tectonic stress, and can easily be crushed into tectonically deformed coal (TDC) under the action of multiple tectonic movements (Cheng and Pan, 2020). Different stress-strain environments can lead to the formation of diverse types of TDCs, which can generally be divided into brittle, brittle-ductile, and ductile deformed sequences according to a structure-genetic classification scheme (Ju and Li, 2009). The various TDCs play different roles in both coalbed methane (CBM) exploration and production and coal and gas outburst. Areas with ductile deformed coals are more prone to gas outburst when developed, and CBM exploitation in such areas is therefore prohibited (Hou et al., 2012). On the other hand, development of brittle deformed coals results in higher gas permeability in favor of CBM exploitation but leads to a lower probability of coal and gas outburst (Jiang et al., 2010).

Coal, being mainly composed of different types of maceral groups, is a highly heterogeneous material at different length scales and cannot be treated as uniform (Sun et al., 2020a). Furthermore, its deformation behavior is believed to be influenced by the distribution of various maceral groups with different mechanical properties, as has been demonstrated in recent studies (Anmin Wang et al.,

2020; Hou et al., 2020). The aforementioned studies on the properties of coal macerals utilized depth-sensing nanoindentation technology (DSNI), which allows the mechanical properties of coal maceral groups to be precisely measured (Kossovich et al., 2019; Anmin Wang et al., 2020; Hou et al., 2020). In contrast to traditional centimeter-scale tests of coal mechanical properties (for example, uniaxial compression, triaxial compression, and tension tests etc.), DSNI is a type of quantitative method for characterizing the nanoscale mechanical properties of substrate materials (Nili et al., 2013). So far, DSNI has already been applied for studying the mechanical properties of lots of materials, including composites, polymers, metals, and crystals (Sankaran et al., 2018; Yuemin Wang et al., 2020; Han et al., 2021; Isik et al., 2022). In recent years, this technology has received increased attention in coal research (Vranjes et al., 2018; Zhang et al., 2018; Sun et al., 2020a; Sun et al., 2020b; Kossovich et al., 2020).

At the small characteristic length scales of nanoindentation, the mechanical properties and deformation characteristics of substrate materials are normally related to the evolution of atomic structure. With the aid of spectral detection, the structural evolution of coal maceral molecules may be connected with their mechanical properties obtained from nanoindentation tests (Anmin Wang et al., 2020). It is believed that the condensation of aromatic structures and breaking of aliphatic structures are some of the main factors controlling the mechanical properties of coal macerals (Anmin Wang et al., 2020; Hou et al., 2020). In other words, mechanical properties of coal macerals are determined to some extent by the differences in inner molecular structure. Hence, the breakthroughs that have been made in micro-scale research regarding the relationships between the mechanical properties and molecular structure of coal macerals have provided a new perspective for evaluating the mechanisms behind the deformation of TDCs based on their heterogeneous maceral distribution.

From a practical point of view, it is difficult to study the indentation process and surface deformation mechanisms of the nanoscale contact area between indenter and substrate materials experimentally. To overcome this challenge, molecular dynamics (MD) simulations have emerged as a powerful tool to simulate nanoindentation in various materials, such as metals, carbonaceous materials, and polymeric materials (Peng et al., 2019; Pascazio et al., 2020; Luu et al., 2021). In the field of coal research, Meng et al. (2020), Meng et al. (2021) carried out MD simulations of coal matrix nanoindentation, which have significantly promoted the understanding of the nanoscale mechanical properties and failure mechanisms of coal. Using MD simulation methods, the interaction mechanism between the indenter and substrate at the nanoscale can be elucidated (Luu et al., 2021). Further, mechanical properties acquired from MD simulations of nanoindentation are often in excellent agreement with experimental results (Valencia et al., 2021; Zhou et al., 2021). Hence, a lot of useful information about the nanoscale deformation mechanism can be obtained from MD simulations of the indention process, including loading and unloading curves and the evolutionary characteristics of the atomic-scale structure.

To the best of our knowledge, there is a lack of research regarding MD simulations of nanoindentation on coal macerals to date. However, the construction methodology for molecular modeling of coal and maceral groups has been well established (Mathews and Chaffee, 2012), which makes the implementation of MD simulations of coal maceral nanoindentation possible. Further, using density gradient centrifugation or heavy-liquid separation methods, high-purity vitrinite can be separated from various coal maceral groups (Yu et al., 2017), and the molecular structures of coal or separated coal maceral groups can be determined using characterization methods such as FTIR, ^{13}C NMR, HRTEM, and XPS (Liu et al., 2019). Finally, 3D molecular models can be constructed using the ACD/CNMR Predictor and Materials Studio software packages (Yu et al., 2017; Liu et al., 2019). Based on these kinds of molecular models (Yu et al., 2019), the present study uses MD simulations to explore the loading and unloading processes in the nanoindentation of vitrinite. The indentation substrate of coal vitrinite was constructed using existing molecular representations of vitrinite. The evolution of molecular configuration around the contact area was revealed and the hardness was calculated according to the simulation results. Furthermore, the influence of vitrinite molecular structures on the mechanical properties of the coal is discussed in-depth. The results from this study are expected to increase the current scientific understanding regarding the nanoindentation of coal maceral groups and the micro-deformation mechanisms of coal vitrinite.

2 SIMULATION METHODOLOGY

2.1 Simulation Model

2.1.1 Vitrinite Representation

The substrate material used for the nanoindentation MD simulations was coal vitrinite. To allow for comparison with the experimental results of Hou et al. (2020), vitrinite separated from medium-low rank coal (with a maximum reflectance of vitrinite, $R_{o,\ max}$, value of 0.9) in Yu et al. (2017) study was adopted, as it has the same coal rank as the samples used in the of Hou et al. (2020) study. The vitrinite was purified using the density gradient centrifugation method, and its molecular structure was characterized using ^{13}C CP/MAS NMR, FTIR, and HRTEM techniques (Yu et al., 2017). Finally, Yu et al. (2017), Yu et al. (2019) acquired an optimized molecular representation of DV-8 coal vitrinite through conducting structural adjustments hundreds of times (**Figure 1A**).

2.1.2 Indentation Substrate

The indentation system was constructed using Materials Studio and the large-scale atomic/molecular massively parallel simulator (LAMMPS). The procedure was as follows: first, 100 vitrinite representations were inserted into a simulation box using the Amorphous Cell module in Materials Studio to build the initial substrate configuration (**Figures 1A, B**). Next, the coordinate data for the initial configuration composed of 41,400 atoms were

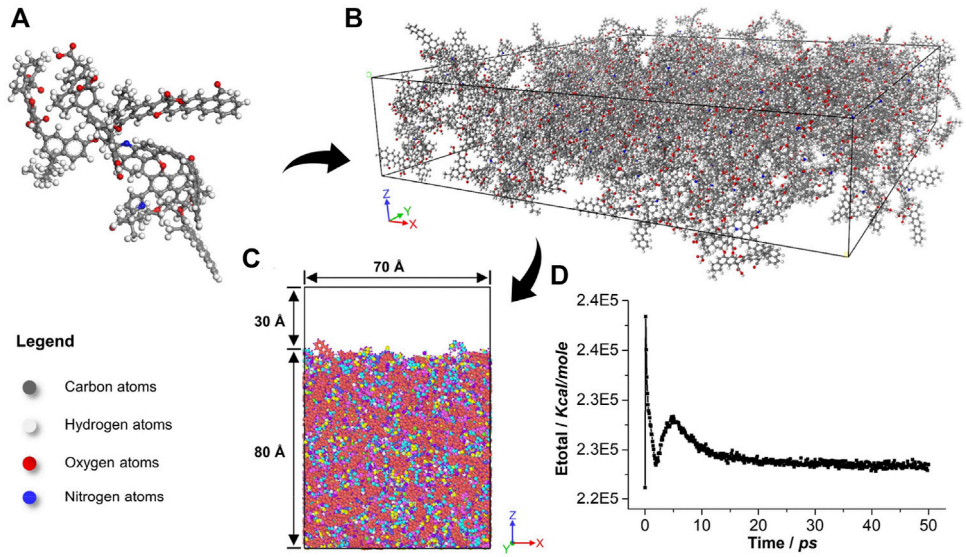

FIGURE 1 | Construction of layered vitrinite configuration using Materials Studio 8.0: **(A)** single vitrinite unit, **(B)** vitrinite configuration composed of 100 single units, **(C)** optimized vitrinite configuration with 30 Å vacuum space (atoms are shown colored by PCFF force field type). **(D)** Total energy of the vitrinite configuration during the optimization process.

transformed to import into LAMMPS. The initial molecular structure was optimized by adding external forces along the *X*- and *Y*-directions, until the density finally reached the target 1.24 g/cm^3. In order to compress the initial structure, periodic boundary conditions were set in the *X*- and *Y*-directions, and a fixed boundary was set in the *Z*-direction. The isothermal-isobaric (NPT) ensemble was used to simulate the compression over a period of 50 ps. The external pressures in the *X*- and *Y*-directions were specified at 45 MPa using the Nose-Hoover pressure barostat, and the box length along the *X*- and *Y*-directions was allowed to change during the simulation. During the compression procedure, the system temperature was thermostatted to 300 K by explicitly rescaling the velocities of atoms.

The relaxation of the layered substrate was performed in the canonical (NVT) ensemble with a Nose-Hoover thermostat at 300 K over a period of 50 ps, at the end of which the total energy of the optimized molecular system reached a relatively stable value (**Figure 1D**). During the relaxation stage, reflect walls were added to the lower and upper boundaries along Z direction of simulation box to restrict the motion of atoms, which could ensure the constant density of substrate system. To provide enough free space for the movement of vitrinite molecules, 30 Å of vacuum space was added above the upper surface of the vitrinite configuration (**Figure 1C**).

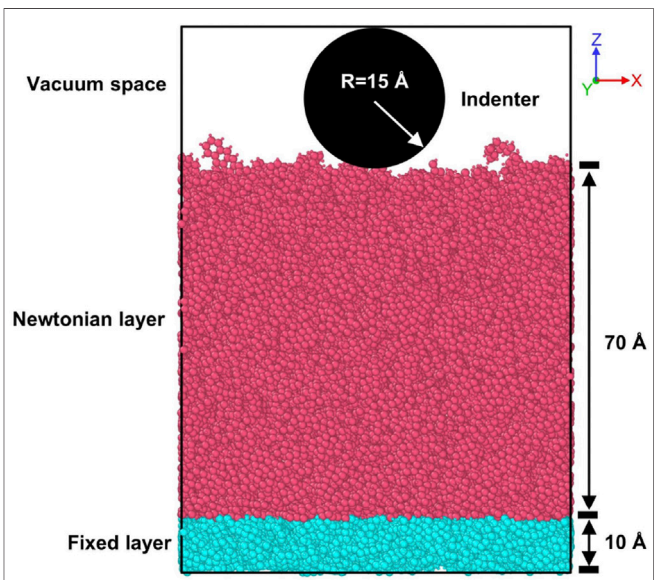

FIGURE 2 | Layered structure of the vitrinite substrate, with the spherical ghost indenter located above.

2.2 Interaction Potentials

The polymer consistent force field (PCFF), one of the consistent family force field developed for synthetic polymers was used to define the atomic interactions in the vitrinite substrate. This force field is widely used for simulating organic polymers and is sufficiently accurate to describe the coal molecular system, which consists of C, H, O, N, and S atoms (Meng et al., 2020). In the PCFF force field, the total energy is composed of valence, cross, and nonbonded energies. The 6/9 Lennard-Jones (LJ) potential was selected to describe the pair interactions between vitrinite atoms, which may be expressed as follows (Sun, 1994):

$$E_{VDW} = \varepsilon_{ij}^{0}\left[2\left(\frac{r_{ij}^{0}}{r_{ij}}\right)^{9} - 3\left(\frac{r_{ij}^{0}}{r_{ij}}\right)^{6}\right](r < r_c) \quad (1)$$

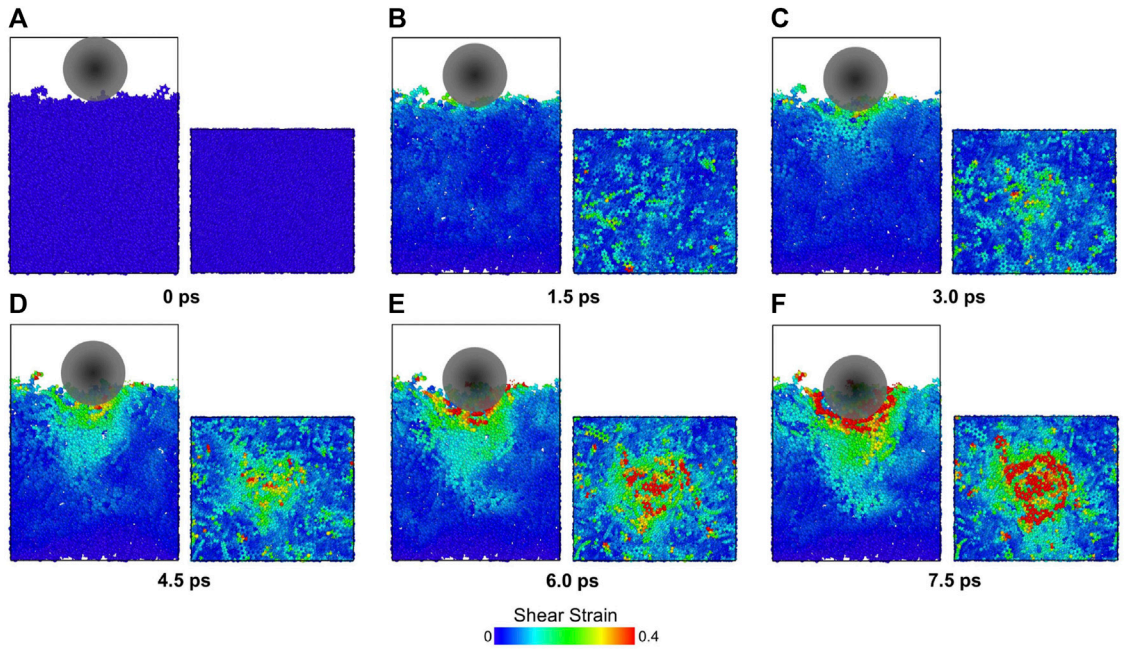

FIGURE 3 | Shear strain distributions of vitrinite atoms during loading at times of **(A)** 0, **(B)** 1.5 ps, **(C)** 3.0 ps, **(D)** 4.5 ps, **(E)** 6.0 ps, and **(F)** 7.5 ps. For each sub-figure, the left- and right-hand images show the front cross-sectional and top views of the vitrinite substrate, respectively.

$$r_{ij}^0 = \left[\frac{\left(r_i^0\right)^6 + \left(r_j^0\right)^6}{2}\right]^{\frac{1}{6}} \tag{2}$$

$$\varepsilon_{ij}^0 = 2\sqrt{\varepsilon_i^0 \cdot \varepsilon_j^0}\left[\frac{\left(r_i^0\right)^3 \cdot \left(r_j^0\right)^3}{\left(r_i^0\right)^6 + \left(r_j^0\right)^6}\right] \tag{3}$$

where E_{VDW} is the nonbonded van der Waals interactions between atoms i and j, r_{ij}^0 is the equilibrium distance between atoms i and j, ε_{ij}^0 is the coefficient of well-depth energy, r_c is the global cutoff distance for LJ interactions, which was set to 10 Å in this study, r_{ij} is the instantaneous distance between atoms i and j, r_i^0 and r_j^0 refer to the equilibrium distances between atoms i and atoms j, respectively, and ε_i^0 and ε_j^0 refer to the well-depth energies of atoms i and j, respectively.

2.3 Implementation of the Indentation

A ghost spherical indenter with a radius of 15 Å was used in the simulations (**Figure 2**). The ghost indenter repels all atoms in the vitrinite substrate, and the repulsive force may be expressed as follows:

$$F(r) = -K(r - R)^2 \tag{4}$$

where K is the specified force constant (which was set to 10 in the simulations), r is the distance between vitrinite atoms and the center of the ghost indenter, and R is the radius of the ghost indenter (= 15 Å).

The bottom layer, with a height of 10 Å, was fixed as a rigid body to avoid vertical translation of the vitrinite substrate (**Figure 2**). Atoms in the Newtonian layer were put into a microcanonical (NVE) ensemble, in which the particles are allowed to move freely as the ghost indenter is pushed into substrate. Atomic motion in the Newtonian layer strictly follows Newton's laws of motion. The loading and unloading rate of the ghost indenter along the Z-direction was set to 200 m/s, and the whole indentation procedure lasted for 7,500 fs. The maximum indentation depth was set to 1.5 nm.

3 RESULTS AND DISCUSSION

3.1 Deformation of Vitrinite During Nanoindentation

The plastic deformation of metallic materials mainly occurs through the dislocation of crystalline structures, while that of amorphous materials such as vitrinite occurs via shear transformation, which refers to the rearrangement of a pack of atoms overcoming the energy barrier (Greer et al., 2013). The rearranged atoms usually normally have very large displacements compared to the surrounding atoms, and the local domain containing rearranged atoms called the shear transformation zone (STZ) (Hua et al., 2020).

The atomic local shear strain, η_i^{Mises}, of each atom i was introduced to quantify the atomic shear deformation of the vitrinite substrate (Shimizu et al., 2007). **Figure 3** shows the shear strain distributions of the vitrinite atoms at different indenter loading stages. The cross-sectional strain distributions reveal that, as the indentation depth increases, the shear strain of the substrate atoms under the ghost indenter

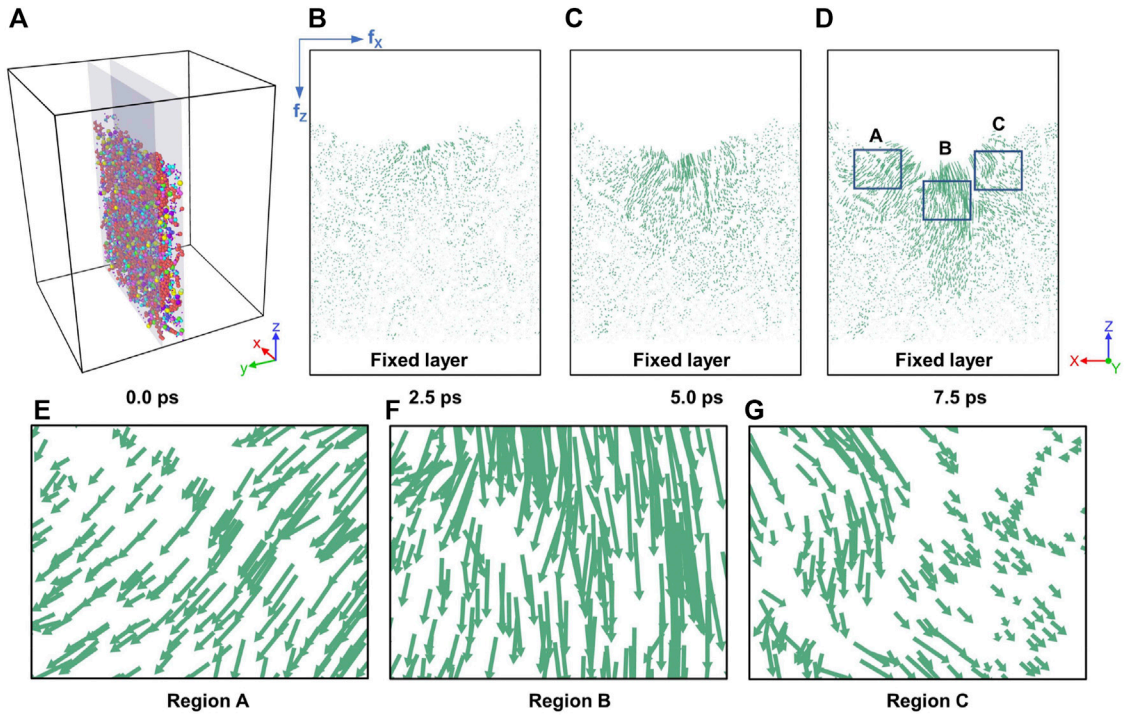

FIGURE 4 | (A) The selected 10 Å vitrinite slice prior to nanoindentation. Displacement vectors of atoms in the 10 Å vitrinite slice during nanoindentation at **(B)** 2.5 ps, **(C)** 5.0 ps, and **(D)** 7.5 ps. Zoomed-in view of the distributions of displacement vectors at regions **(E)** A, **(F)** B, and **(G)** C at 7.5 ps as marked in **(D)**.

rapidly increases, propagating from the contact region to the outside of the indenter. In addition, the overhead view of the vitrinite substrate indicates that the shear strain of atoms expands rapidly from the center to periphery as the indentation depth increases. The proliferation of the STZ is mainly concentrated directly below the ghost indenter, indicating that the shear strain spreads directly into the interior of the vitrinite substrate. Essentially, the proliferation of the STZ represents the spreading and rearrangement of vitrinite atoms, which allows the stress-strain energy produced from elastic loading to be released.

3.2 Motion of Vitrinite Atoms During Nanoindentation

To determine the motion of atoms in the vitrinite substrate, the atomic displacement vectors in a vertical slice with a width of 10 Å were calculated using the OVITO software package (Version 3.4.4) (**Figure 4**). The green arrows in **Figure 4** show the directions of vitrinite atom motion, and the length of the green line represents the displacement of the atom. The results show that as the loading depth of the ghost indenter increases, the displacement vectors of vitrinite atoms around the indenter gradually lengthen under the effect of the repulsive forces between the substrate and the indenter (**Figures 4A–D**). Further, the magnitudes and directions of the displacement vectors vary with location. At region B, atoms directly below the ghost indenter move vertically downwards during the indentation process, which indicates that the substrate atoms in this region are mainly subjected to the force along the *Z*-direction (f_Z). On the other hand, the substrate atoms at regions A and C move downwards at an angle to the vertical, indicating that the atoms in these regions are subjected to the forces along both the *X*- and *Z*-directions (f_X and f_Z). The displacements of atoms at region B are also much larger than those at A and C, which illustrates significant variation in the magnitudes of the forces acting on atoms at different locations.

Given the variations in displacement seen in **Figure 4**, the local substrate atoms around ghost indenter can be roughly subdivided into six distinct regions (**Figure 5**), with the atoms in each region moving in more or less the same direction, but in a different direction to those in the other regions. Molecular chains or atoms of neighboring regions slip at the region boundary, leading to the formation of shear bands. **Figure 5** shows that the displacement of vitrinite atoms in regions I, II, and III is generally much larger than that in other regions (Lin et al., 2021). This is likely due to the fact that, in the initial indentation stage, atoms in these regions are the first to be subjected to repulsive forces and start moving. These atoms then squeeze the ones in regions IV, V, and IV, causing those peripheral atoms to move in the following indentation stage. However, the directions of motion of the squeezed atoms diverge due to the heterogenous molecular structures and inner stress differentiation within the substrate, resulting in slippage at the region boundaries, viz. the shear bands.

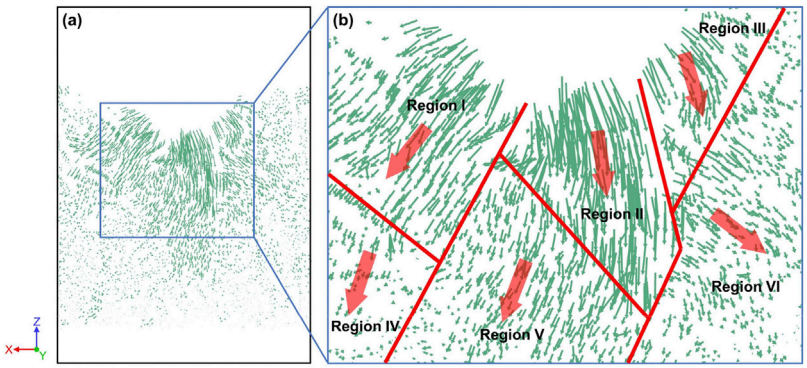

FIGURE 5 | (A) Displacement vectors of atoms in the 10 Å vitrinite slice at 7.5 ps as shown in **Figure 4**. **(B)** Zoomed-in view of the region highlighted by the blue square in **(A)**, showing the distribution of six subdivided displacement regions. The red arrows represent the average displacement directions of the atoms in each region.

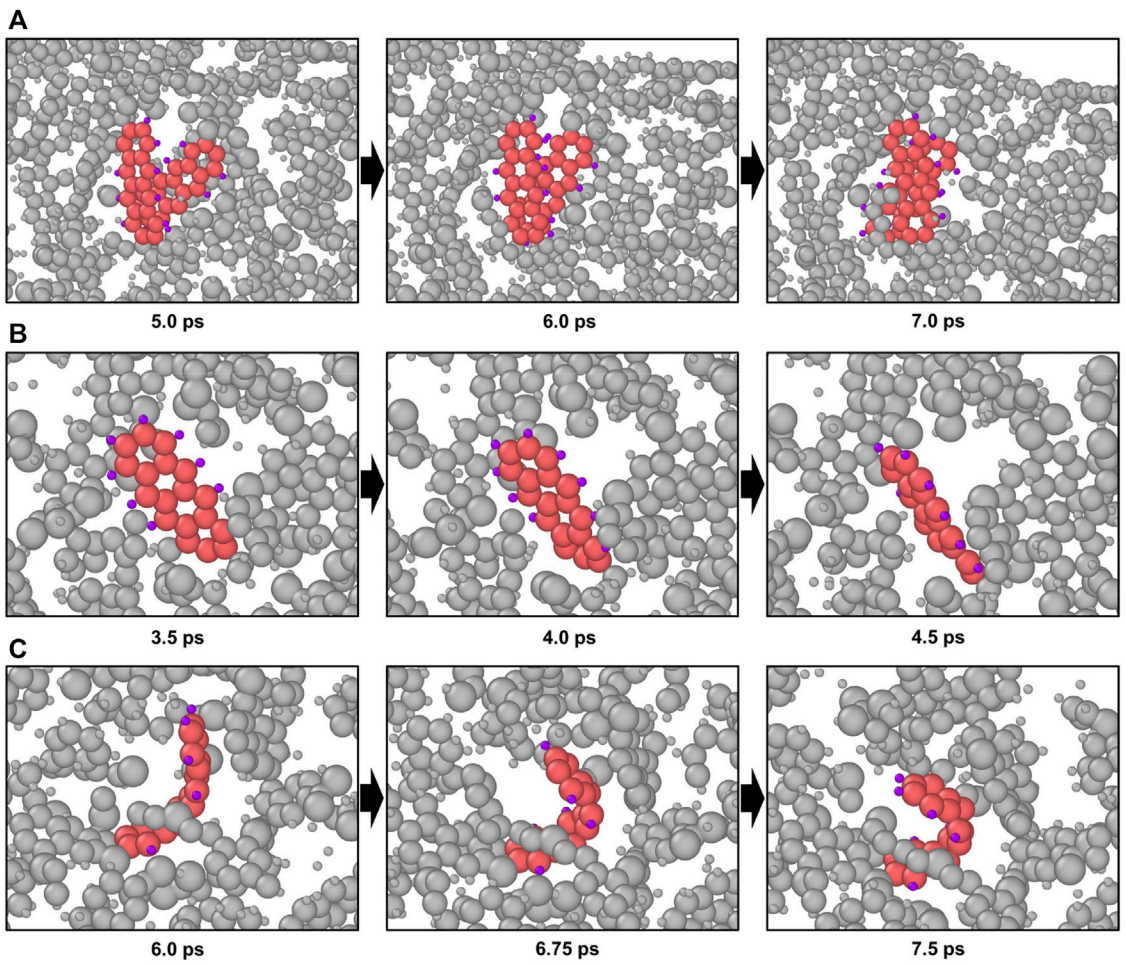

FIGURE 6 | Different adjustment behaviors of vitrinite molecular chains: **(A)** sliding between aromatic structure, **(B)** reorientation of aromatic lamella, **(C)** bending of aromatic chains.

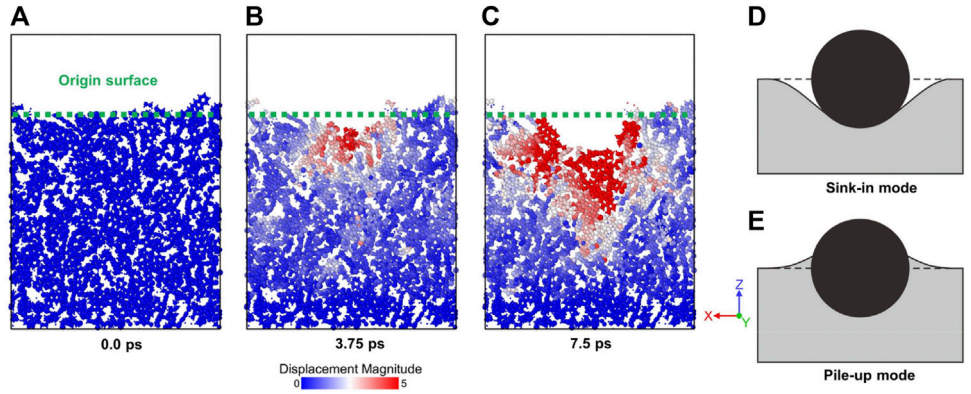

FIGURE 7 | Surface morphologies of vitrinite substrate: **(A–C)** Variation of surface morphologies at different loading stages. Schematic images of **(D)** sink-in and **(E)** pile-up surface morphologies.

3.3 Comparison Between Coal Deformation and Nanoindentation

The response of coal molecular structures to tectonic stress-induced deformation, which is similar to the molecular variation during indenter loading process, has been well-researched (Cao et al., 2007; Pan et al., 2015; Song et al., 2018). In terms of the plastic deformation of coal induced by tectonic stress, the motion of molecular chains is the most significant deformation mechanism (Liu and Jiang, 2019), which also leads to the formation of STZs in TDCs. During the indentation process, the adjustment of molecular chains is another important deformation mechanism of the vitrinite substrate. At the initial loading stage, the emergence of the STZ in vitrinite substrate may be initiated in the "weak spots" (atoms with larger free volume) in the vitrinite substrate (Wang et al., 2010). Under the effect of shear stress, the STZ begins to propagate via the adjustment of vitrinite molecular chains. The motion of vitrinite atoms in distinct regions (**Figure 5**) indicated that the adjustment of molecular chains is due to factors such as sliding between aromatic layers, reorientation of aromatic lamella, and bending of aromatic chains (**Figure 6**), which is similar to the molecular variations seen for the plastic deformation of coal (Ju et al., 2014; Han et al., 2017).

Moreover, the development of structural defects, which mainly includes various types of point defects, is promoted in TDCs (Pan et al., 2017; Song et al., 2019). Similarly, for the indentation of vitrinite substrate, the STZ also appears be a kind of point defect, with a greater degree of structural disorder and a larger free volume (Greer et al., 2013). Apart from the development of defects, nanocrystallization also appears in the shear bands during nanoindentation (Kim et al., 2002), which is similar to the aromatization of ductile deformed coal (Hou et al., 2012). During the vitrinite indentation process, sliding between the aromatic layers can enhance the degree of stacking of the vitrinite molecular structures (**Figure 6A**); hence, it is evident that the atomic evolution of the vitrinite structure is consistent with that of TDCs.

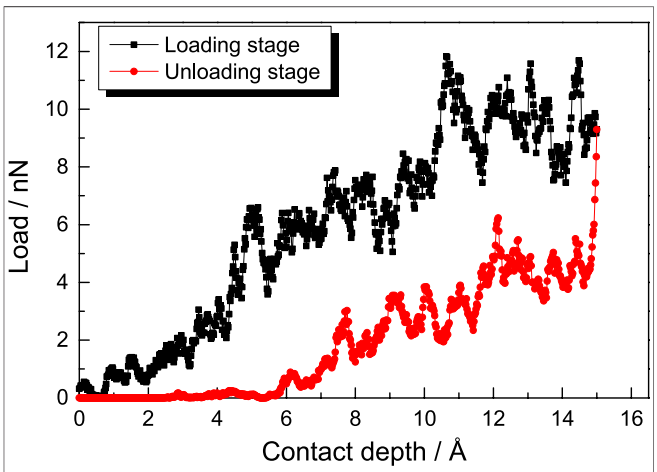

FIGURE 8 | The relationship between the loading force and contact depth.

3.4 Surface Morphology

A 10 Å slice extracted from the middle of the simulation box (as shown in **Figure 4A**) was used to identify the surface morphology of the vitrinite substrate (**Figures 7A–C**). Following penetration by the indenter, different substrates tend to show one of there will be two main modes of indentation behavior, either sink-in or pile-up modes (Hou et al., 2020) (as illustrated in **Figures 7D,E**). In this case, **Figure 7** shows that the surface morphology of vitrinite atoms after penetration is inclined towards the sink-in mode, which is consistent with previous experiments (Hou et al., 2020). The surface morphology of substrate materials is actually determined by the density of substrate atoms (Hua et al., 2020), with a higher atomic density of substrate material likely to lead to greater atomic pile-up around the indenter. Vitrinite is of lower atomic density and has a loose molecular structure relative to metals and other materials. Consequently, there is enough free space for vitrinite atoms to move and for molecular chains to adjust, which leads to the sink-in type surface.

3.5 Mechanical Properties of Vitrinite Obtained From Nanoindentation Simulations

Figure 8 shows the mechanical properties of vitrinite obtained from the simulations. As the contact depth increases, the repulsive forces between the indenter and the vitrinite atoms are enhanced. In the loading process, the load-depth curve (**Figure 8**) is serrated, which may be due to the shear transformation of vitrinite substrate (Schuh and Nieh, 2003). Serrations on the load-depth curve correspond to sudden load drops of vitrinite indentation. For each serration, at the initial elastic loading stage, vitrinite atoms are not able to overcome the motion energy barrier; therefore, the loading force continues to increase. Once the generated strain energy crosses the energy barrier, a pile of atoms under the indenter is able to move freely, giving rise to the formation of the STZ. As the loading displacement is constant rate, the activation of shear transformation leads directly to a decreasing in the load drop, which corresponds to fluctuation in the load-depth curve. In the unloading process, a sudden drop of load appears at the initial unloading stage (**Figure 8**), which is caused by the high unloading velocity (Zhu and Fang, 2012). The repulsive force between the indenter and substrate atoms disappears once the distance between substrate atoms and the center of spherical indenter is larger than the indenter radius. Therefore, the unloading of indenter with high velocity directly leads to the separation between substrate atoms and indenter, which results in the sudden drop of load.

The hardness, H, which is a commonly-used parameter to characterize the resistant ability to allow hard objects press into (Zhu and Fang, 2012), is defined as the ratio of load force to the projected contact area when the indentation depth is maximum, as follows:

$$H = \frac{F}{A_c} \tag{5}$$

where F is the load of ghost indenter, and A_c is the projected contact area of the ghost indenter embedded into the substrate material. For a spherical ghost indenter, A_c is calculated as follows (Qiu et al., 2014):

$$A_c = \pi(2R - h)h \tag{6}$$

where R is the radius of ghost indenter and h is the indentation depth. According to **Eqs. 5**, **6**, the simulated hardness of coal vitrinite at indentation depth of 1.5 nm is calculated to be 1.31 GPa. Experiments have shown that the vitrinite hardness in coal with similar rank was in the range of 0.52–0.72 GPa (Hou et al., 2020), which is a little lower than the simulated value from the present study. For nano-scale simulations, the simulated hardness of vitrinite be influenced by factors such as the indentation size effects, temperature, indenter radius, and loading rate (Luu et al., 2021; Valencia et al., 2021). However, as there is basically no existing literature regarding the influence of the aforementioned factors on coal vitrinite hardness, it is hard to clarify exactly which of these factors led to the overestimation of the hardness in the current simulations. This issue will be examined in more detail in a future study.

4 CONCLUSION

In this study, the nanoindentation of vitrinite was simulated using a molecular dynamics (MD) approach. During the nanoindentation process, some of the vitrinite atoms overcome the energy barrier to produce a range of motion, including sliding, bending, and reorientation of vitrinite molecular chains, resulting in the formation of STZs. The formation of STZs is the most significant deformation mechanism of vitrinite substrate under the action of repulsive forces. From the distribution of atomic displacements in the vitrinite substrate, the presence of six subdivided regions was identified, with slippage at the region boundaries that can produce shear bands. In the shearing transformation zone, the molecular structural evolution is similar to the variations seen in TDC deformation, including formation structural defects and stacking of the aromatic structures. The surface morphology of the vitrinite substrate was found to be of the sink-in type, which is consistent with experimental results. In addition, the mechanical properties calculated from the nanoindentation simulations were also similar to experimental results. Hence, the MD simulation results from this paper help in understanding the atomic response to the vitrinite nanoindentation process and the deformation mechanism of the vitrinite substrate. The clarification of the nano-scale deformation mechanism of coal macerals obtained from this work provides valuable insight, with a sound theoretical basis, into coal deformation behavior under the influence of coal heterogeneity.

DATA AVAILABILITY STATEMENT

The original contributions presented in the study are included in the article/Supplementary Material, further inquiries can be directed to the corresponding authors.

AUTHOR CONTRIBUTIONS

LH write and financially support this paper; HC design the research scheme and write this paper; SY correct this paper.

FUNDING

This work was supported by the National Natural Science Foundation of China (Grant number 42102221), the Natural Science Foundation of Anhui Province (Grant number 2108085QD167), the Independent Research Fund of the State Key Laboratory of Mining Response and Disaster Prevention and Control in Deep Coal Mines (Grant number SKLMRDPC20ZZ10), and the Scientific Research Starting Foundation for the Introduced Talents of Anhui University of Science and Technology.

REFERENCES

Anmin Wang, A., Cao, D., Wei, Y., and Liu, Z. (2020). Macromolecular Structure Controlling Micro Mechanical Properties of Vitrinite and Inertinite in Tectonically Deformed Coals-A Case Study in Fengfeng Coal Mine of Taihangshan Fault Zone (North China). *Energies* 13 (24), 6618. doi:10.3390/en13246618

Cao, D., Li, X., and Zhang, S. (2007). Influence of Tectonic Stress on Coalification: Stress Degradation Mechanism and Stress Polycondensation Mechanism. *Sci. China Ser. D* 50 (1), 43–54. doi:10.1007/s11430-007-2023-3

Cheng, Y., and Pan, Z. (2020). Reservoir Properties of Chinese Tectonic Coal: A Review. *Fuel* 260, 116350. doi:10.1016/j.fuel.2019.116350

Greer, A. L., Cheng, Y. Q., and Ma, E. (2013). Shear Bands in Metallic Glasses. *Mater. Sci. Eng. R: Rep.* 74 (4), 71–132. doi:10.1016/j.mser.2013.04.001

Han, Y., Wang, J., Dong, Y., Hou, Q., and Pan, J. (2017). The Role of Structure Defects in the Deformation of Anthracite and Their Influence on the Macromolecular Structure. *Fuel* 206, 1–9. doi:10.1016/j.fuel.2017.05.085

Han, R. Q., Song, H. Y., and An, M. R. (2021). Atomic Simulation of Interaction Mechanism between Dislocation and Graphene in Graphene/aluminum Composites. *Comput. Mater. Sci.* 197, 110604. doi:10.1016/j.commatsci.2021.110604

Hou, Q., Li, H., Fan, J., Ju, Y., Wang, T., Li, X., et al. (2012). Structure and Coalbed Methane Occurrence in Tectonically Deformed Coals. *Sci. China Earth Sci.* 55 (11), 1755–1763. doi:10.1007/s11430-012-4493-1

Hou, C., Jiang, B., Liu, H., Song, Y., and Xu, S. (2020). The Differences of Nanoscale Mechanical Properties Among Coal Maceral Groups. *J. Nat. Gas Sci. Eng.* 80, 103394. doi:10.1016/j.jngse.2020.103394

Hua, D., Ye, W., Jia, Q., Zhou, Q., Xia, Q., Shi, J., et al. (2020). Molecular Dynamics Simulation of Nanoindentation on Amorphous/amorphous Nanolaminates. *Appl. Surf. Sci.* 511, 145545. doi:10.1016/j.apsusc.2020.145545

Isik, M., Gasanly, N. M., and Rustamov, F. A. (2022). Determination of Mechanical Properties of Bi12TiO20 Crystals by Nanoindentation. *Mater. Sci. Semiconductor Process.* 140, 106389. doi:10.1016/j.mssp.2021.106389

Jiang, B., Qu, Z., Wang, G. G. X., and Li, M. (2010). Effects of Structural Deformation on Formation of Coalbed Methane Reservoirs in Huaibei coalfield, China. *Int. J. Coal Geol.* 82 (3-4), 175–183. doi:10.1016/j.coal.2009.12.011

Ju, Y., and Li, X. (2009). New Research Progress on the Ultrastructure of Tectonically Deformed Coals. *Prog. Nat. Sci.* 19 (11), 1455–1466. doi:10.1016/j.pnsc.2009.03.013

Ju, Y., Luxbacher, K., Li, X., Wang, G., Yan, Z., Wei, M., et al. (2014). Microstructural Evolution and Their Effects on Physical Properties in Different Types of Tectonically Deformed Coals. *Int. J. Coal Sci. Technol.* 1 (3), 364–375. doi:10.1007/s40789-014-0042-1

Kim, J.-J., Choi, Y., Suresh, S., and Argon, A. S. (2002). Nanocrystallization during Nanoindentation of a Bulk Amorphous Metal alloy at Room Temperature. *Science* 295 (5555), 654–657. doi:10.1126/science.1067453

Kossovich, E. L., Borodich, F. M., Epshtein, S. A., Galanov, B. A., Minin, M. G., and Prosina, V. A. (2019). Mechanical, Structural and Scaling Properties of Coals: Depth-Sensing Indentation Studies. *Appl. Phys. A, Mater. Sci. Process.* 125 (3), 1–15. doi:10.1007/s00339-018-2282-1

Kossovich, E. L., Borodich, F. M., Epshtein, S. A., and Galanov, B. A. (2020). Indentation of Bituminous Coals: Fracture, Crushing and Dust Formation. *Mech. Mater.* 150, 103570. doi:10.1016/j.mechmat.2020.103570

Lin, J., Jiang, F., Xu, X., Lu, J., Tian, Z., Wen, Q., et al. (2021). Molecular Dynamics Simulation of Nanoindentation on C-Plane Sapphire. *Mech. Mater.* 154, 103716. doi:10.1016/j.mechmat.2020.103716

Liu, H., Jiang, B., Song, Y., and Hou, C. (2019). The Tectonic Stress–Driving Alteration and Evolution of Chemical Structure for Low- to Medium-Rank Coals—By Molecular Simulation Method. *Arab J. Geosci.* 12 (23), 1–16. doi:10.1007/s12517-019-4909-8

Liu, H., and Jiang, B. (2019). Stress Response of Noncovalent Bonds in Molecular Networks of Tectonically Deformed Coals. *Fuel* 255, 115785. doi:10.1016/j.fuel.2019.115785

Luu, H.-T., Dang, S.-L., Hoang, T.-V., and Gunkelmann, N. (2021). Molecular Dynamics Simulation of Nanoindentation in Al and Fe: On the Influence of System Characteristics. *Appl. Surf. Sci.* 551, 149221. doi:10.1016/j.apsusc.2021.149221

Mathews, J. P., and Chaffee, A. L. (2012). The Molecular Representations of Coal - A Review. *Fuel* 96, 1–14. doi:10.1016/j.fuel.2011.11.025

Meng, J., Niu, J., Xia, J., and Kan, L. (2020). Study on Mechanical Properties and Failure Mechanisms of Coal at the Nanometer Scale. *Chin. J. Rock Mech. Eng.* 39 (01), 84–92. (In Chinese with English abstract). doi:10.13722/j.cnki.jrme.2019.0659

Meng, J., Cao, Z., Zhang, S., Wang, C., and Nie, B. (2021). Micro-mechanical Properties and Damage Mechanisms of Coal under Cyclic Loading: A Nanoindentation experiment and Molecular Dynamics Simulation. *Mol. Simulation*, 1–12. doi:10.1080/08927022.2021.2015070

Nili, H., Kalantar-Zadeh, K., Bhaskaran, M., and Sriram, S. (2013). *In Situ* nanoindentation: Probing Nanoscale Multifunctionality. *Prog. Mater. Sci.* 58 (1), 1–29. doi:10.1016/j.pmatsci.2012.08.001

Pan, J., Zhu, H., Hou, Q., Wang, H., and Wang, S. (2015). Macromolecular and Pore Structures of Chinese Tectonically Deformed Coal Studied by Atomic Force Microscopy. *Fuel* 139, 94–101. doi:10.1016/j.fuel.2014.08.039

Pan, J., Lv, M., Bai, H., Hou, Q., Li, M., and Wang, Z. (2017). Effects of Metamorphism and Deformation on the Coal Macromolecular Structure by Laser Raman Spectroscopy. *Energy Fuels* 31 (2), 1136–1146. doi:10.1021/acs.energyfuels.6b02176

Pascazio, L., Martin, J. W., Bowal, K., Akroyd, J., and Kraft, M. (2020). Exploring the Internal Structure of Soot Particles Using Nanoindentation: A Reactive Molecular Dynamics Study. *Combustion and Flame* 219, 45–56. doi:10.1016/j.combustflame.2020.04.029

Peng, C., Zeng, F., Yuan, B., and Wang, Y. (2019). An MD Simulation Study to the Indentation Size Effect of Polystyrene and Polyethylene with Various Indenter Shapes and Loading Rates. *Appl. Surf. Sci.* 492, 579–590. doi:10.1016/j.apsusc.2019.06.173

Qiu, C., Zhu, P., Fang, F., Yuan, D., and Shen, X. (2014). Study of Nanoindentation Behavior of Amorphous alloy Using Molecular Dynamics. *Appl. Surf. Sci.* 305, 101–110. doi:10.1016/j.apsusc.2014.02.179

Sankaran, R. P., Ozdol, V. B., Ophus, C., Kacher, J., Gammer, C., Govindjee, S., et al. (2018). Multiscale Analysis of Nanoindentation-Induced Defect Structures in Gum Metal. *Acta Materialia* 151, 334–346. doi:10.1016/j.actamat.2018.03.048

Schuh, C. A., and Nieh, T. G. (2003). A Nanoindentation Study of Serrated Flow in Bulk Metallic Glasses. *Acta Materialia* 51 (1), 87–99. doi:10.1016/s1359-6454(02)00303-8

Shimizu, F., Ogata, S., and Li, J. (2007). Theory of Shear Banding in Metallic Glasses and Molecular Dynamics Calculations. *Mater. Trans.* 48 (11), 2923–2927. doi:10.2320/matertrans.mj200769

Song, Y., Jiang, B., and Han, Y. (2018). Macromolecular Response to Tectonic Deformation in Low-Rank Tectonically Deformed Coals (TDCs). *Fuel* 219, 279–287. doi:10.1016/j.fuel.2018.01.133

Song, Y., Jiang, B., and Qu, M. (2019). Macromolecular Evolution and Structural Defects in Tectonically Deformed Coals. *Fuel* 236, 1432–1445. doi:10.1016/j.fuel.2018.09.080

Sun, C., Li, G., Zhang, S., Xu, J., and Yang, H. (2020). Mechanical and Heterogeneous Properties of Coal and Rock Quantified and Mapped at the Microscale. *Appl. Sci.* 10 (1), 342. doi:10.3390/app10010342

Sun, C., Li, G., Gomah, M. E., Xu, J., and Sun, Y. (2020). Creep Characteristics of Coal and Rock Investigated by Nanoindentation. *Int. J. Mining Sci. Tech.* 30 (6), 769–776. doi:10.1016/j.ijmst.2020.08.001

Sun, H. (1994). Force Field for Computation of Conformational Energies, Structures, and Vibrational Frequencies of Aromatic Polyesters. *J. Comput. Chem.* 15 (7), 752–768. doi:10.1002/jcc.540150708

Valencia, F. J., Santiago, J., González, R. I., González-Arrabal, R., Ruestes, C., Perez Díaz, M., et al. (2021). Nanoindentation of Amorphous Carbon: A Combined Experimental and Simulation Approach. *Acta Materialia* 203, 116485. doi:10.1016/j.actamat.2020.116485

Vranjes, S., Misch, D., Schöberl, T., Kiener, D., Gross, D., and Sachsenhofer, R. F. (2018). Nanoindentation Study of Macerals in Coals from the Ukrainian Donets Basin. *Adv. Geosci.* 45, 73–83. doi:10.5194/adgeo-45-73-2018

Wang, Y.-C., Wu, C.-Y., Chu, J. P., and Liaw, P. K. (2010). Indentation Behavior of Zr-Based Metallic-Glass Films via Molecular-Dynamics Simulations. *Metall. Mat Trans. A.* 41 (11), 3010–3017. doi:10.1007/s11661-010-0358-4

Yu, S., Yan-Ming, Z., and Wu, L. (2017). Macromolecule Simulation and CH4 Adsorption Mechanism of Coal Vitrinite. *Appl. Surf. Sci.* 396, 291–302. doi:10.1016/j.apsusc.2016.10.127

Yu, S., Bo, J., and Fengjuan, L. (2019). Competitive Adsorption of CO2/N2/CH4 onto Coal Vitrinite Macromolecular: Effects of Electrostatic Interactions and Oxygen Functionalities. *Fuel* 235, 23–38. doi:10.1016/j.fuel.2018.07.087

Yuemin Wang, Y., Shang, L., Zhang, P., Yan, X., Zhang, K., Dou, S., et al. (2020). Measurement of Viscoelastic Properties for Polymers by Nanoindentation. *Polym. Test.* 83, 106353. doi:10.1016/j.polymertesting.2020.106353

Zhang, Y., Lebedev, M., Al-Yaseri, A., Yu, H., Xu, X., Sarmadivaleh, M., et al. (2018). Nanoscale Rock Mechanical Property Changes in Heterogeneous Coal after Water Adsorption. *Fuel* 218, 23–32. doi:10.1016/j.fuel.2018.01.006

Zhou, J., Jiao, Z., Zhang, J., and Zhong, Z. (2021). Nanoindentation of Single-crystal and Polycrystalline Yttria-Stabilized Zirconia: A Comparative Study by Experiments and Molecular Dynamics Simulations. *J. Alloys Compd.* 878, 160336. doi:10.1016/j.jallcom.2021.160336

Zhu, P. Z., and Fang, F. Z. (2012). Molecular Dynamics Simulations of Nanoindentation of Monocrystalline Germanium. *Appl. Phys. A.* 108 (2), 415–421. doi:10.1007/s00339-012-6901-y

Conflict of Interest: The authors declare that the research was conducted in the absence of any commercial or financial relationships that could be construed as a potential conflict of interest.